Motion and coalescence of a pair of bubbles rising side by side

Toshiyuki SANADA(Corresponding Author)
Department of Mechanical Engineering
Shizuoka University
3-5-1 Johoku, Naka-ku, Hamamatsu, Japan 432-8561
ttsanad@ipc.shizuoka.ac.jp

Ayaka SATO
Department of Mechanical Engineering Science
Kyushu University
744 Motooka, Nishi-ku, Fukuoka, Japan 819-0395
sato@mech.kyushu-u.ac.jp

Minori SHIROTA
Research Center for Hydrogen Use and Storage,
National Institute of Advanced Industrial Science and Technology,
744 Motooka, Nishi-ku, Fukuoka, Japan 819-0395
shirota-minori@aist.go.jp

Masao WATANABE
Department of Mechanical and Space Engineering
Hokkaido University
N13 W8, Kita-ku, Sapporo, Japan 060-8628
masao.watanabe@eng.hokudai.ac.jp

Motion and coalescence of a pair of bubbles rising side by side

ABSTRACT

Bouncing and coalescence of a pair of slightly deformed bubbles rising side by side in a quiescent liquid are experimentally studied. The trajectories and shapes of the bubbles are investigated in detail by using a high-speed video camera. The wakes of bubbles are visualized by using a photochromic dye that is colored with UV light irradiation. We observe that the patterns of the trajectories of rising bubbles are strongly dependent on the Reynolds number. When the Reynolds number is over the critical region, two bubbles approach each other and then collide. After the collision, two types of motions are observed—coalescence and bouncing. We investigate the critical Reynolds number and Weber number over which the bubbles bounce. In the definitions of these numbers, we use vertical velocity, instead of horizontal one, as the characteristic velocity. We clarify that the critical Weber number is around 2 regardless of the Morton number. The critical Reynolds number decreases with an increase in the Morton number. Moreover, the visualization of the wake of bubbles enables us to observe the vortex separation from the rear surface of the bubbles on collision. We find that the vortex separation from the rear of bouncing bubbles causes a decrease in the rising velocity and an increase in the horizontal speed after their collision. We also observe that the behavior of repeatedly bouncing bubbles is significantly influenced by the wake instability of a single bubble rather than by the bubble-bubble interaction. By applying an existing model for spherical bubble-bubble interaction, we clarify that the revised model accurately describes the trajectory of a pair of slightly deformed bubbles using the restitution coefficient and velocity fluctuation from the experimental results.

Key Words: Bubble, Coalescence, Bouncing, Rising velocity, Wake

1. INTRODUCTION

Liquid flows containing bubbles are used in many industrial applications such as heat exchangers and bubble-column reactors. The structure of a bubbly flow changes considerably depending on various effects such as the interactions between bubbles, the velocity fluctuation of individual bubbles, bubble coalescence or bouncing, and so on. In order to predict bubbly flow behavior accurately, it is necessary to have sufficient knowledge of fluid dynamics, particularly with regard to the abovementioned issues.

The behavior of a single bubble (Duineveld, 1995) and that of a pair of bubbles with fluid dynamical interactions (Kok, 1993b) have already been studied in detail under the approximation of potential flow (Kok, 1993a). However, the construction of a theoretical model of bubble behavior in a bubble cloud or bubble cluster is not a straightforward extension of the abovementioned studies, mainly due to the complicated interaction effects among bubbles. The model of elastic collision among contacting bubbles, which is derived under the potential flow assumption, results in a formation of horizontal bubble clusters (Sangani and Didwania, 1993; Smereka, 1993). The horizontal clusters are observed experimentally (Zenit et al., 2001; Figueroa-Espinoza and Zenit, 2005; Takagi et al., 2008) by adding a small amount of electrolyte or surfactant in order to reduce the bubble coalescence. In the usual bubble column, however, coalescence frequency occurs. It is recognized that a more specific model that describes the interactions among bubbles, such as velocity fluctuations and bubble collisions, and that is based on fluid dynamic examination should be developed for a more accurate prediction of the behavior of bubbles (Yurkovetsky and Brady, 1996; Spelt and Sangani, 1998; Moctezuma, et al., 2005). In the bubble-wall interaction, hydrodynamic force, bouncing are experimentally investigated (Tsao and Koch, 1994; 1997; Takemura and Magnaudet, 2003) and modeled (Kushch et al., 2002). In addition, de Vries et al. (2002) experimentally studied the collision of spherical bubbles with a vertical wall. They showed that the model that describes spherical bubble motion under the potential flow approximation with experimentally obtained velocity fluctuations successfully predicts the motion of a single bubble that bounces against the wall. However, there is lack of experimental knowledge for the bubble-bubble interaction.

When designing gas-liquid reaction devices, it is essential that not only the bubble size distribution but also the gas-liquid contact areas should be estimated. In other words, the bubble number density, which is the number of bubbles of specified diameters in unit volume, should be evaluated. The bubbles generated in gas-liquid reaction devices undergo repeated coalescence and breakup as they contact with each other due to mutual interactions that occur as they rise in these devices. It should be noted that the coalescence of a pair of bubbles of the same diameter decreases the bubble

surface area by approximately 20%; consequently, several consecutive repetitions of coalescence reduce the total bubble surface area by more than half. Therefore, bubble coalescence conditions should be accurately evaluated in order to estimate the gas-liquid contact area. Unfortunately, this bubble coalescence and breakup process is not appropriately treated in most of the contemporary numerical predictions.

Kirkpatric and Lockett (1977) studied bubble coalescence by observing the collision between a rising bubble and a free surface. They clarified that a bubble either bounces against a free surface in the case of large approaching velocity or coalesces otherwise. Chesters and Hofman (1982) numerically studied the liquid film between the free surfaces of a pair of bubbles. They showed that a significant amount of pressure rise in the thin liquid film causes the characteristic shape that is referred to as a "dimple" and the bouncing of bubbles in the case of sufficiently large approaching velocity. Duineveld (1998) observed the behavior of a pair of bubbles that collide with each other and then coalesce or bounce in super-purified water. He showed that there exists a critical Weber number, which was based on the horizontal velocity of a pair of bubbles, for the criteria of coalescence. Lehr et al. (2002) also proposed the bubble coalescence/bouncing model: a large approaching velocity causes bubble bouncing, while a small approaching velocity leads to coalescence. On the other hand, Sanada et al. (2005) showed, by numerical analysis (DNS) of the flow field of a rising bubble colliding with a free surface, that the flow structure in the liquid film between the bubble and free surface and the bubble wake structure are dominant factors that determine whether the bubbles coalesce with or bounce against a free surface.

In this study, we experimentally study the motion of a horizontally aligned pair of rising bubbles; in particular, we determine the conditions of the boundary at which the bubbles either coalesce or bounce. We discuss this boundary by using bubble vertical velocity, which is one of the dominant factors that determines bubble wake. We also investigate the relation between the velocity fluctuations at the centers of mass of the bubbles and bubble wake with the help of the flow visualization technique using a photochromic dye. We classify the motion of a pair of bubbles observed in the experiment as follows: (1) coalescence of two bubbles, (2) bouncing of bubbles and larger separation than an initial distance between bubbles, and (3) repetitive collision of a pair of bubbles without coalescence. Finally, we discussed the application validity of the viscous potential model (Kok, 1993a; de Vries, 2002) to the slightly deformed bubbles rising side by side.

2. EXPERIMENTAL APPARATUS AND PROCEDURE

2.1. EXPERIMENTAL APPARATUS

In this study, two kinds of experiments were performed—bubble motion visualization and bubble wake visualization. We generated a pair of bubbles, whose diameters were accurately controlled, by using a bubble generator activated by a pulsed pressure wave (Shirota et al., 2008） into quiescent liquid, which was either silicone oil (Shin-Etsu Chemical Co., Ltd., Silicone fluids KF-series) or purified water. A pair of nitrogen gas bubbles was simultaneously generated and released from two orifices with a diameter of 0.3 mm, which were drilled on the side of a single nylon tube. This tube, one end of which was sealed, was placed at the bottom of a transparent acrylic-walled tank. Figure 1 shows the schematic diagram of the experimental apparatus for bubble motion visualization and a detailed view of the bubble generator. A high-speed video camera (NAC, Hi-Dcam 8000s, 500Hz ~ 2000Hz) with backlighting was used to capture the images. This camera was linearly raised when a high spatial resolution was required. The translational motion of this camera was so controlled that the upward velocity was synchronized with that of the rising bubble.

In order to visualize the wake of bubbles, we used a 25 ppm silicone oil solution of photochromic dye (1,1,3 – Trimethylindolino-6'-nitrobenzopyrylospiran) . In the normal state, the photochromic dye solution is clear and colorless. Irradiated ultraviolet (UV) light activates the dye, turning it dark blue. Figure 2 shows the schematic of the experimental apparatus for the bubble wake visualization. UV sheet light having a height of approximately 10 mm and width of approximately 50 mm was supplied by a UV light projector (Moritex Corp., MUV-250U-L). A pair of bubbles was generated immediately after UV sheet light illuminated the part of the liquid just above the bubble generation orifice in order to activate the photochromic dye. Once the bubble passed across the colored part of the liquid, the bubbles were accompanied by some activated dye tracers. In this manner, the flow structure behind a pair of rising bubbles was visualized. The visualized wake was recorded by a high-speed video camera (Vision Research, Inc., Phantom V.4.2, 1000Hz). By using this method, the free surface condition holds. The detail of this visualization method is in Sanada et al. (2007). In our early study (Sanada, et. al., 2008), we have studied the effect of water purity on the bubble motion by comparing two cases; extremely clean water, the purity of which was achieved by extremely careful and repetitive pre-cleaning (using of course the super purified water) of the observation tank and water supplying system, and just super purified water with no special pre-cleaning for the experimental tank. We have obtained results that there are no differences between two cases in the Reynolds number range of the present study. This result of our early study leads us to use purified water, not extremely purified water, in this study.

The initial distance between bubbles lies in the range from 2.2 to 5.0 mm, while the bubble radius ranges from 0.41 to 0.95 mm. The physical properties of purified water (W), silicone oil (K0.65~K10), and silicone oil with photochromic dye mixture (M) are listed in Table 1. The dimensionless Reynolds number (*Re*), Weber number (*We*), and Morton number (*Mo*) are defined by equations 1, 2, and 3, respectively.

$$Re = \frac{2rw}{\nu} \tag{1}$$

$$We = \frac{2\rho r w^2}{\sigma} \tag{2}$$

$$Mo = \frac{g\nu^4\rho^3}{\sigma^3} \tag{3}$$

Where, ρ and ν denote the density and kinematic viscosity of the liquid, σ the surface tension, *w* the bubble rise velocity, *r* the bubble radius and g the gravitational acceleration.

2.2. IMAGE PROCESSING

All images were taken by a high-speed video camera. From these images, the radius, rising velocities, and centers of mass of the bubbles were calculated. First, redundant elements such as the nylon tube and color shading of the background were removed from the original images. Next, the noise in the image was filtered out by using a median filter. In order to obtain the bubble outline, we binarized the images using Otsu's method (Otsu, 1980), which calculates the threshold automatically by using the histogram of the image. Finally, the derived bubble outline was reconstructed smoothly by applying Fourier descriptions. We calculated the radius *r*, which is a periodic function of θ with period π. This function $r(\theta)$ can be written as

$$r(\theta) = A_0 + \sum_{n=1}^{N} A_n \cos n\theta + \sum_{n=1}^{N} B_n \sin n\theta . \tag{4}$$

By solving this equation with an iterative method to cause the terms A_1 and B_1 to be zero, the centers and velocities of the bubbles were computed.

In order to strengthen the contrast of the image visualizing bubble wake, gamma correction was done using the MATLAB image processing toolbox.

3. EXPERIMENTAL RESULTS

3.1. BUBBLE TRAJECTORY

First, we classify the direction of the mutual interaction force on a pair of bubbles rising side by side. Legendre et al. (2003) numerically studied the motion of a pair of spherical rising bubbles aligned horizontally by using DNS and showed that the direction of relative motion of the bubbles changes primarily in accordance with the *Re* number. They found that the transitional *Re* number was in the range of $30 < Re < 100$. When *Re* is greater than the transitional *Re*, the bubbles approach each other since the potential force dominates due to the sufficiently thin boundary layer developed on the bubble surface. On the other hand, for a smaller value of *Re*, the bubbles separate from each other since the viscous force dominates due to the vortical flow developed around the bubbles.

Typical examples of motion of a pair of bubbles are shown in Fig. 3. Figure 3(a) shows the results of $Re = 16$. In this case, the bubbles rose separating from each other after they were generated, mainly due to the repulsive forces that resulted from the asymmetry of the vorticity development around a bubble, as shown by Legendre et al. (2003) in their numerical study. On the contrary, the bubbles approached each other after they were generated and then collided in all cases from Figs. 3(b) to 3(d). After the collision, the two bubbles coalesced in the case of $Re = 209$, as shown in Fig. 3(b), while the bubbles bounced in the case of $Re = 221$, as shown in Fig. 3(c). It should be added that in case (c) the separation distance between the bounced bubbles becomes greater than the initial distance and that they rose upward rectilinearly. Moreover, in the case of $Re = 361$, two bubbles repeatedly attracted and bounced against each other, as shown in Fig. 3(d).

We confirmed that two rising bubbles approach each other after they were generated for a high value of *Re*. Next, we discuss both the coalescence and bouncing of a pair of bubbles rising in this range of *Re*.

3.2 CRITERIA OF COALESCENCE

We discuss the boundary between coalescence and bouncing of a pair of rising bubbles using the vertical velocity, which is one of the important dominant factors in bubble wake development, as the characteristic velocity in the definition of both *Re* and *We*. First, we observed whether two bubbles rising side by side form stable separation distance, coalesce, or bounce under the various experimental conditions by changing both *Re* and *Mo*. The results are shown in

Fig. 4, with *Re* and log(*Mo*) as the ordinate and abscissa, respectively. In Fig. 4, the crosses represent the experimental conditions under which the bubbles were observed to bounce, and the open circles denote coalescence. When the boundaries between coalescence and bouncing were defined by *Re*, they varied in accordance with the liquid chosen. The critical Reynolds number were found in the range of approximately 540 to 590 in experiments using purified water, represented by W. The critical Re in experiments using silicone oils K0.65, K1, K1.5, and K2 were approximately 240, 210, 160, and 110, respectively; the critical *Re* decreased with an increase in the liquid *Mo*.

Next, we discuss the effects of *We* on the boundaries. The same experimental results as obtained in Fig. 4 are plotted in Fig. 5 with *We* and log(*Mo*) as the ordinate and abscissa, respectively. The critical *We* range approximately form 1.8 to 2.1 in the W experiments. In the experiments using silicone oils K0.65, K1, K1.5, and K2 the critical *We* were approximately 2.1, 2.0, 2.1, and 1.9, respectively. It should be noted that the vertical velocity *w* is used as the characteristic velocity in the definition of *We* in this study. By using *We* thus defined, the boundaries between coalescence and bouncing were found for a *We* of approximately 2.0 for all cases of *Mo*. We conclude that the most essential parameters for classifying the boundaries between coalescence and bouncing of a pair of rising bubbles is *We*, which is based on the bubble vertical velocity *w*, rather than the horizontal velocity, as the characteristic velocity.

In the next section, we proceed to study bubble bouncing in further detail. We discuss the bubble motion observed by using a high-speed video camera whose translational motion was controlled and upward velocity was synchronized with that of the rising bubble. We also discuss the wake developed behind the rising pair of bubbles by flow visualization using photochromic dye.

3.3. MOTION AND WAKE OF BOUNCING OR COALESCENCE BUBBLES

We first discuss the typical patterns of motion of a pair of bubbles, as observed in the experiments. We also discuss the wake interaction by investigating the bubble wake visualized by using an activated photochromic dye. The following three patterns were observed: (1) coalescence of a pair of bubbles, (2) bouncing and larger horizontal separation than the initial distance of a pair of bubbles, and (3) repetitive collision of a pair of bubbles without coalescence.

The visualization of the wakes of a pair of bubbles of patterns 2 and 3 were also carried out. Table 2 shows the experimental parameters of typical bubble motions. The roles of bubble wake in bubble motion for each typical pattern are discussed below.

3.3.1 CASE OF COALESCENCE BUBBLES (PATTERN 1)

First, we discuss the coalescence of a pair of bubbles. Figure 6 shows the bubble trajectories and velocity changes. Figure 7 shows the shapes of a pair of bubbles before and after coalescence. A pair of bubbles approached each other, after which the bubble rise velocities decreased and the approach velocity of the bubbles (u_{left}–u_{right}) increased. The two bubbles took some finite time to coalesce after they contacted with each other, as shown in Figure 7. The bubbles first contacted at a height of 8.5 mm and 0.035 s after the generation, and then they finally coalesced at a height of 10.5 mm and 0.042 s. During and after coalescence, a decrease in the bubble rise velocity was observed, although the diameter of the coalesced bubble increased, i.e., the buoyancy increased. Further, during the first period of velocity fluctuation after coalescence (Fig. 6 (b)), the rise velocity, *w*, reached the smallest value—approximately 165 mm/s—which was approximately 20% lower than that before coalescence. After coalescence, the coalesced bubble rose with shape oscillations, as shown in Figs. 6 and 7. One period of rise velocity fluctuation after coalescence, measured from (a) to (b) as indicated in Fig. 6, was approximately 7.0 ms.

We assume that the *k*-th order mode of the natural oscillation of a spherical bubble may provide a good approximation to that of a slightly deformed bubble with equilibrium radius r_{eq}, expressed as following;

$$\omega_{0,k}^2 = (k-1)(k+1)(k+2)\frac{\sigma}{\rho r_{eq}^3} \cdot \qquad (5)$$

From Eq. (5), the period of the second mode shape oscillation T_2 is expressed as

$$T_2 = \frac{2\pi}{\sqrt{12\dfrac{\sigma}{\rho_l r_{eq}^3}}} \cdot \qquad (6)$$

By substituting the values of the experimental parameters r_{eq} = 0.70 mm and σ = 16.9 mN/m in Eq. (6), the period of the second mode shape oscillation was calculated as T_2 = 7.4 ms, which was close to the value of one period of rise velocity fluctuation after coalescence. This second mode shape oscillation may have induced the rise velocity fluctuation.

It should be emphasized that the rise velocity of the coalesced bubble was approximately 20% lower than that before coalescence and that the coalesced bubble continued to rise with second mode shape oscillation.

3.3.2 CASE OF BOUNCING BUBBLES (PATTERN 2)

Next, we discuss the motion of a pair of bounced bubbles whose horizontal separation was larger than the initial distance. Figure 8 shows the bubble trajectories and velocity change. Figure 9 shows the visualized motion of bubble and wake. As clearly shown in Fig. 8, the rise velocities decreased significantly immediately after the bubbles bounced. In this case, the rise velocity dropped down to almost 50% at collision. This result is similar to that obtained by de Vires (2002), who observed bubble bouncing on a vertical glass wall. The most characteristic feature of the bubble-bubble collision process is that it took a finite amount of contact time and not just an instant for two bubbles to collide. It took approximately 5 ms from the onset to the completion of contact. This contact time is shown in Figure 8; the bubbles began to touch each other at (a) and separated from each other at (b). This observed result differs from the commonly used bubble-bubble collision models, which assume instant elastic collision. It should be emphasized that the maximum values for the relative horizontal velocities before and after contact were 25 mm/s and 57 mm/s, respectively. This result shows that the bubbles collide with superficial superelasticity, which is caused by the surrounding liquid motion, mainly due to the bubble wake. It should be noted that this super-elastic bouncing is superficial. We also observed the reduction in the vertical velocity from 220 mm/s to 100mm/s This result clearly shows that the horizontal super-elastic bouncing is superficial since the magnitude of the velocity is reduced by 48 %.

Figure 9 shows that the wakes behind a pair of bubbles bounced off each other. During bubble collision, the wakes collided with each other, and the bubbles bounced immediately, as shown in Fig. 9(a). In this case, the decrease in the vertical velocity is not significant. In some cases, on the other hand, the rise velocity decreases significantly; typical pictures for this case is shown in Fig. 9 (b). Here the bubbles first collide and then the wakes enter between bubbles during bubble deformation (bubble contact time). Subsequently, the wakes overtake the bubbles. From the visualization image, we conclude that the superficial superelasticity bouncing and decrease in rise velocity are caused by the motion of the surrounding liquid, particularly the bubble wake. As shown in the previous section, we showed that the criteria for the bouncing are expressed by the critical Weber number, which is based on the vertical velocity of bubble, to be around 2. It is widely recognized that the Weber number is the most important parameter to determine bubble shape. In addition, the bubble shape has been shown to be the dominant factor for the bubble wake development, as Zenit and Magnaudet (2008) clarified that the onset of path instability of bubble depends significantly on the bubble shape aspect ratio, while

it is well known that the path instability is closely related to the bubble wake development. Therefore the Weber number itself is recognized as the dominant parameter for the wake development.

This discussion leads us to propose an assumption that the bubble wake is the dominant factor for bubble bouncing. Our early study of the interaction between rising bubble and free surface also showed that the bubble wake is the important factor to determine bubble bouncing on the free surface (Sanada et al., 2005). However, our measurements of bubble wake in this study are restricted to the qualitative observation, mainly due to the limit of the present experimental method. The more detailed discussion of the mechanism of bubble bouncing is our future work.

3.3.2 CASE OF REPEATED BOUNCING BUBBLES (PATTERN 3)

We discuss the repetitive collision of a pair of bubbles without coalescence. Figure 10 shows the bubble trajectories and velocity changes of right-hand side bubble in the case of pattern 3, and the motion of a single rising bubble with non rectilinear motion, denoted by pattern 3', for comparison. (Note that the initial horizontal position of the single bubble was shifted to x = 6.0 mm for clarity.) In the case of a pair of bubbles (pattern 3), the decrease in the rise velocity was considerably smaller than that obtained in patterns 1 and 2. The most striking result is that both the period and amplitude of repetitive bouncing of the pair of bubbles are in excellent agreement with those of a single rising bubble with non rectilinear motion. Therefore, it is concluded that the wake instability, as observed in a single rising bubble with non rectilinear motion, is more dominant than the interaction between bubbles in the motion of bubbles with repetitive collision. Figure 11 shows the wake of a pair of bubbles that separated from each other without contacting. The double-thread wake clearly observed in Fig. 11(a) (Mougin and Magnaudet, 2002) and the horseshoe-shaped wake clearly observed in Fig. 11(b) (Lunde and Perkins, 1997) support the aforementioned conclusion that the motion of a pair of bubbles with changing direction without contact is dominated by the wake instability, as observed in a single rising bubble.

4. COMPARISON WITH A SIMPLE MODEL

Kok (1993a) proposed a theoretical model of motion of a pair of interacting bubbles at a high Reynolds number. His model was derived with potential flow approximation. The drag acting on bubbles was calculated from the viscous dissipation rate. Thereafter, de Vries et al. (2002) simplified Kok's model to study a bubble bouncing on a vertical wall. We recognized that the application of this model is not restricted to bubble bouncing on the wall; it can also encompass the bubble-bubble interactions. It should be noted that this model is only applicable when the assumption of both the spherical shape of bubbles and planar motion of bubbles holds true.

As previously stated, the bubble bouncing cannot be described by the simplified model; hence, additional conditions should be set (de Vries 2002). The bubble slides along the wall when the Weber number is less than the critical Weber number, while it bounces on the wall when the Weber number is equal to or greater than the critical Weber number, where the critical Weber number is 0.165. We use the following equation set derived by de Vries et al. (2002) to study the motion of a pair of bubbles,

$$\rho V_B \frac{d M_z \dot{z}}{\mathrm{d}t} = F_z$$
$$\rho V_B \frac{d M_x \dot{x}}{\mathrm{d}t} = \frac{1}{2}\rho V_B \left[\dot{z}^2 \frac{d M_z}{d x} + \dot{x}^2 \frac{d M_x}{d t} \right] + F_x \tag{7}$$

where

$$M_z = 1 + \frac{3}{16}\left(\frac{r_{eq}}{x}\right)^3, M_x = 1 + \frac{3}{8}\left(\frac{r_{eq}}{x}\right)^3, F_z = 2\rho g V - D_z, F_x = -D_x$$
$$D_z = 24\pi\mu r_{eq}\dot{z}\left[1 + \frac{1}{8}\left(\frac{r_{eq}}{x}\right)^3\right], D_x = 24\pi\mu r_{eq}\dot{x}\left[1 + \frac{1}{4}\left(\frac{r_{eq}}{x}\right)^3\right]$$

where, M_z and M_x are the added mass coefficients, F_z and F_x are the external force terms, and D_z and D_x are the drag forces acting on the pair of spheres.

We compared our experimental results with those obtained by the simplified theoretical model. We studied only the planar motion of the bubbles. The bubbles rose in a plane spanned by half the initial separation and vertical axis. The horizontal coordinate of the bubble was defined from the vertical axis through the midpoint of the initial bubble separation. Both the horizontal and vertical coordinates of the bubble at an arbitrary time were calculated by those of the bubbles located on the opposite side of the vertical axis, as if the vertical axis were the wall surface in the planar motion

of the bubble. As mentioned above, Eq. (7) was derived under the assumption that the bubble has a spherical shape. However, the bubbles observed in our experiment were ellipsoidal with the minor axis aligned in the direction of bubble motion. As the deformation of the bubbles significantly alters both the drag and an added mass force, we considered the following four factors due to bubble deformation in the model. These factors influence the motion of bubbles: (1) the increase in the drag due to bubble deformation, (2) the finite contact time on bubble collision, (3) superficial superelastic collision, and (4) the lift force due to bubble deformation.

First, we discuss the increase in drag. The drag acting on a deformed bubble, which is ellipsoidal with the minor axis aligned in the direction of the bubble motion, is larger than the drag on a spherical bubble (Moore, 1965). Hence, in order to approximate the drag on a deformed bubble by using a spherical bubble model, the equivalent radius of the deformed bubble was corrected so that the terminal velocity, which is also defined as the characteristic velocity, calculated by the model agrees with that obtained in the experiment.

Our experimental results in Fig. 8 show, as discussed in the previous section, that it takes some finite contact time from the onset to the completion of bubble contact. On the contrary, the model derived by de Vries et al. (2002) assumed that the bubbles bounce instantaneously. In order to take the finite contact time into account, we used the actual contact time measured from our experiment.

In the model of de Vries et al. (2002), the bubble collides instantaneously against a wall while maintaining a spherical shape; further, the bubble has perfectly elastic collision in a horizontal direction. However, as discussed in the preceding chapter, as the wake was detached from the rear of the bubbles immediately after bubble collision, the magnitude of the velocity of the bubbles in the horizontal direction after bouncing was larger than that before contact. We observed the superficial superelastic collision of bubbles in the horizontal direction. We considered this superficial superelastic collision effect by calculating a restitution coefficient and substituting it in the model.

Finally, it was clarified that the motion of a pair of bubbles rising side by side is similar to the zigzagging/spiraling motion of a single rising bubble. It is commonly recognized that the zigzagging/spiraling motion is induced by a lift force acting on the bubble. Keeping this in mind, we evaluate the lift force due to bubble deformation by comparing the experimental results with the theoretical results with or without considering the lift force.

These four factors were applied to the three different patterns of motion observed in the experiments (patterns 1, 2, and 3). First, we discuss the coalescence of bubbles. Figure 12 shows the trajectories and the velocity changes obtained in our experiment along with those obtained by the theoretical model. As discussed previously, in order to obtain the appropriate terminal velocity as obtained in the experiment, we substituted the modified bubble radius, which was 10%

smaller than that measured in the experiment, in the model. Both the trajectories and the velocity changes calculated by this model were in excellent agreement with the experimental results. It was found that the approaching process of a pair of bubbles was described accurately by the potential flow theory, as shown by Kok (1993b).

Secondly, we discuss the motion of a pair of bounced bubbles whose final horizontal separation was greater than the initial distance. Figure 13 shows the comparison of the revised model with the experimental result. As in the abovementioned case, the radius of the bubble was modified. Further, the finite contact time and restitution coefficient obtained from the experimental results were applied to the model. As shown in Figure 13, both the bubble trajectory and velocity changes obtained from the revised model were in good agreement with the experimental results. This suggests that the motions of the bubbles can be predicted, if we obtain the appropriate model for the velocity fluctuations of bubbles (e.g. restitution coefficients, velocity decrease, coalescence condition and so on.).

Finally, we discuss the repetitive collision of a pair of bubbles without coalescence. In the previous section, we showed that the motions of bubbles with repetitive collision were dominantly influenced by the wake instability, as observed in a single bubble zigzagging/spiraling motion, rather than the interactions between bubbles. Hence, we added lift force, which causes the zigzagging/spiraling motion, to the model. The lift force derived by de Vries et al. (2002) expressed as follows:

$$F_z = 2\rho g V - D_z + 2L\cos\beta$$

$$F_x = -D_x - 2L\sin\beta \qquad (8)$$

$$L \approx \frac{\pi\rho U_T^2 r_{eq}^2}{13}$$

where β is the angle made by the path with the horizontal. de Vries et al. (2002) added the terms $2L\cos\beta$ and $-2L\sin\beta$ to the external force term to represent the lift forces. In Fig. 14, without the lift force, three times of bubble bouncing was calculated; this value is different from the experimental result. Even taking the lift force into account, the model can not be applicable to the motions of bubbles observed in the experiments. This result indicates that the wake instability acting on an isolated bubble mainly influences the repetitive bouncing motion of the bubbles. In order to predict the bubble behavior quantitatively, it is necessary to construct more appropriate models.

By applying the four factors due to the bubble deformation to the model, we discussed the applicability of the model to the deformed bubbles that rise side by side. On using the experimental results in the condition of bouncing, the revised model and the experimental result were found to be in good agreement. We conclude that if bubble behaviors such as the restitution coefficient and velocity fluctuation and so on can be modeled properly, it will be possible to predict the bubble behavior more accurately.

5. CONCLUSION

We experimentally studied the motion and wake of a pair of bubbles rising side by side in silicone oil and water. On comparing the results obtained experimentally with those obtained from the theoretical model, we make the following conclusions.

・The velocity of a pair of bubbles rising side by side decreases after coalescence, and the coalesced bubble rises vertically with shape oscillations of the second order mode.

・The velocities of the bubbles decrease by as much as 50% when the bubbles rising side by side bounce off each other. Immediately after bubble collision, a large amount of fluid was observed to intrude the space between the bubbles, which resulted in the bubbles moving in a direction away from each other.

・The motion of the bubbles is dominantly influenced by the path instability of the rising bubble, as observed in the case of a single rising bubble with zigzag/spiraling motion, when a pair of bubbles bounce repeatedly.

・On using the experimental results in the condition of bouncing, it was found that the model derived by de Vires et al. (2002) can be used to predict the motion of bubbles accurately.

ACKNOWLEDGEMENTS

We would like to express our gratitude to S. Sato and K. Sugihara for their cooperation in the experiments, and P. Stanovsky for valuable discussion. This work is supported in part by Grant-in-Aid for Scientific Research (B) 17360082, and by the JSPS-ASCR Joint Research Project by the Japan Society for the Promotion of Science.

REFERENCES

Chesters, A. K., Hofman, G., 1982. Bubble coalescence in pure liquids. Appl. Sci. Res. 38, 353–361.

Duineveld, P. C., 1995. The rise velocity and shape of bubbles in pure water at high Reynolds number. J. Fluid Mech. 292, 325–332.

Duineveld, P. C., 1998. Bouncing and coalescence of bubble pair rising at high Reynolds number in pure water or aqueous surfactant solutions. Appl. Sci. Res. 58, 409–439.

Figueroa-Espinoza, B., Zenit, R., 2005. Clustering in high Re monodispersed bubbly flows. Phys. Fluids. 17, 091701.

Kirkpatrick, R. D., Lockett, M. J., 1974. The influence of approach velocity on bubble coalescence. Chem. Eng. Sci. 29, 2363–2373.

Kok, J. B. W., 1993a. Dynamics of gas bubbles moving through liquid: part I: theory. Eur. J. Mech. B 12, 515–540.

Kok, J. B. W., 1993b. Dynamics of gas bubbles moving through liquid: part II: experiments. Eur. J. Mech. B 12, 541–560.

Kushch, V. I., Sangani, A. S., Spelt, P. D. M., Koch, D. L., 2002. Finite-weber-number motion of bubbles throuth a nearly inviscid liquid. J. Fluid Mech. 460, 241-280.

Legendre, D., Magnaudet, J., Mougin, G., 2003. Hydrodynamic interactions between two spherical bubbles rising side by side in a viscous liquid. J. Fluid Mech. 497, 133–166.

Lehr, F., Millies M., Mewes, D., 2002. Bubble-size distributions and flow fields in bubble columns. AIChE J. 48, 2426–2443.

Lunde, K., Perkins, R. J., 1997. Observations on wakes behind spheroidal bubbles and particles. Proc. ASME-FED Summer Meeting, FEDSM97-3530.

Moctezuma, M. F., Lima-Ochoterena, R., Zenit, R., 2005. Velocity fluctuations resulting from the interaction of a bubble with a wall. Phys. Fluids. 17, 098106.

Moore, D. W., 1965. The rise velocity of distorted gas bubbles in a liquid of small viscosity. J. Fluid Mech. 23, 749–766.

Mougin, G., Magnaudet, J. 2002. Path instability of a rising bubble. Phy. Rev. Lett. 88, 014502.

Otsu, H., 1980. An automatic threshold selection method based on discriminant and least squares criteria. Trans. Electro. Commun. Eng. Jpn D. J63, 349–356.

Sanada, T., Watanabe, M., Fukano, T., 2005. Effects of viscosity on coalescence of a bubble upon impact with a free

surface. Chem. Eng. Sci. 60, 5372–5384.

Sanada, T., Watanabe, M., Fukano, T., 2006. Interaction and coalescence of bubbles in stagnant liquid. Multiphase Sci. Tech. 18, 155–174.

Sanada, T., Shirota, M., Watanabe, M., 2007. Bubble wake visualization by using photochroic dye. Chem. Eng. Sci. 62, 7264-7273.

Sanada T., Sugihara K., Shirota M., Watanabe M., 2008. Motion and drag of single bubbles in super-purified water, Fluid Dynamics Research, vol.40, 534-545.

Sangani, A. S., Didwania, A. K., 1993. Dynamic simulations of flow of bubbly liquids at large Reynolds numbers. J. Fluid Mech. 250, 307–337.

Shirota, M., Sanada, T., Sato A., Watanabe, M., 2008. Formation of a submillimeter bubble from an orifice using pulsed acoustic pressure waves in gas phase. Phys. Fluids. 20, 043301.

Smereka, P., 1993. On the motion of bubbles in a periodic box. J. Fluid Mech. 254, 79–112.

Spelt, P. D. M, Sangani, A. S., 1998. Properties and averaged equations for flows of bubbly liquid. Appl. Sci. Res. 58, 337–386.

Takagi, S., Ogasawara, T., Matsumoto, Y., 2008. The effects of surfactant on the multiscale structure of bubbly flows. Philosophical Transaction of The Royal Society A. 366, 2117-2129.

Takemura, F., Magnaudet, J., 2003. The transverse force on clean and contaminated bubbles risng near a vertical wall at moderate Reynolds number. J. Fluid Mech. 495, 235-253.

Tsao, H. K., Koch, D. L., 1994. Collisions of slightly deformable, high Reynolds number bubbles with short-range repulsive forces. Phys. Fluids. 6, 2591-2605.

Tsao, H. K., Koch, D. L., 1997. Observation of high Reynolds number bubbles interacting with a rigid wall. Phys. Fluids. 9, 44-56.

de Vries, A.W.G., Biesheuvel, A., van Wijngaarden, L., 2002. Notes on the path and wake of a gas bubble rising in pure water. Int. J. Multiphase Flow 28, 1823–1835.

van Wijngaarden L., 1993. The mean rise velocity of pairwise-interacting bubbles in liquid. J. Fluid Mech. 251, 55–78.

Zenit, R., Koch, D. L., Sangani, A. S., 2001. Measurements of the average properties of a suspension of bubbles rising in a vertical channel. J. Fluid Mech. 429, 307-342.

Zenit, R., Magnaudet, J., 2008. Path instability of rising spheroidal air bubbles: A shape-controlled process. Phys. Fluids. 20, 061702.

APPENDIX

It should be noted that the Weber number based on the relative velocity between bubbles has been popularly used (Chesters and Hoffman, 1982; Tsao and Koch, 1994; Duineveld, 1998) to discuss the bubble bouncing/coalescence in the context of the film drainage: however, we used the bubble rising velocity w for the definition of dimensionless number Re and We, as inspired by the analysis by Takemura and Magnaudet (2003). They used Reynolds number based on the vertical velocity of rising bubble, in order to study a bubble bouncing on a wall.

The dominating idea that motivated us to use the Weber number based on the bubble rising velocity is that the bubble wake, which intrude between bubbles at the collision, play a crucial role for the bubble bouncing or coalescence. It is therefore quite natural to use the characteristic velocity that determines the flow structure of wake, that is, vertical velocity, rather than relative horizontal velocity: hence we use the Weber number based on the vertical velocity.

The additional reason why we have used the Weber number based on the bubble rising velocity is that we have found that the use of the Weber number based on the relative horizontal velocity is irrelevant in the present experiment, due to the extreme difficulty in the experimental measurement of the relative horizontal velocity "ON" the bubble collision. The origin of this difficulty is explained as follows. From the potential flow theory, the lift coefficients acting on spherical bubbles rising side by side is expressed as follows (Kok, 1993; Legendre et al., 2003);

$$C_L = -6s^{-4}\left(1 + s^{-3} + \frac{16}{3}s^{-5} + \frac{3}{4}s^{-6} + 15s^{-7} + \frac{22}{3}s^{-8} + \frac{65}{2}s^{-9} + \frac{767}{9}s^{-10} + O(s^{-11})\right) \qquad \text{(A1)}$$

Here, s is the dimensionless separate distance between two bubbles. The leading order of the lift coefficients is s^{-4}. It is thus clear that the horizontal velocity rapidly increases when the bubbles approach closer. Figure A1 shows the time evolution of bubble distance and approaching velocity u. As shown in this graph, the approaching velocity rapidly increases when the bubbles approach to each other. In our experiments on the criteria for bubble bouncing, the recording rate of a high speed camera was 500Hz. Figure A2 shows the bubble shape deformation images obtained by this frame rate during bubble collision. It is clearly understood that it is extremely difficult task to determine "when bubbles collided". These experimental results have leaded us to conclude that the approaching velocity u cannot be uniquely defined in our present measurements.

For example, the approaching velocity increases under the condition of 500Hz and 7812Hz as shown in Fig. A3. The cross marks shown in Fig. A3 are the velocities measured 500Hz, and velocities on these marks are 77, 85, 95 and 110 mm/s, respectively.

These variations in the approaching velocities result in the huge differences in the Weber numbers. On the other hand, the bubble vertical velocity is almost constant just before the bubble collision as shown in Fig. A4. This experimental result also has leaded us to use the bubble vertical velocity for the definition of dimensionless numbers.

FIGURE & TABLE CAPTIONS

Figure 1. Experimental apparatus on bubble motion visualization

Figure 2. Experimental apparatus on bubble wake visualization

Figure 3. Trajectory of a pair of bubbles rising in a quiescent liquid

(a) s=1.8 mm, Re=16

(b) s=2.2 mm, Re=209

(c) s=2.2 mm, Re=221

(d) s=2.5 mm, Re=361

Figure 4. Criteria of coalescence of *Re* (W:Water, K:Silicone oil)

Figure 5. Criteria of coalescence of *We* (W:Water, K:Silicone oil)

Figure 6. Trajectory and vertical/horizontal velocity of a pair of bubbles (pattern 1)

Figure 7. Shape change of coalescence bubble from left to right, line by line to the bottom (Δt=0.5msec)

Figure 8. Trajectory and vertical/horizontal velocity of a pair of bubbles (pattern 2)

Figure 9. Wake of bouncing of bubbles (Δt=4msec)

Figure 10. Trajectory and vertical/horizontal velocity of a pair of bubbles (pattern 3)

Figure 11. Wake of pair of bubbles (Δt=10msec)

Figure 12. Comparison of experiment with model (pattern 1)

Figure 13. Comparison of experiment with model (pattern 2)

Figure 14. Comparison of experiment with model (pattern 3)

Table 1 Properties of liquid (W: Water, K: Silicone oil, M: Silicone oil with photochromic dye mixture)

Table 2 Experimental parameters of each bubble pattern

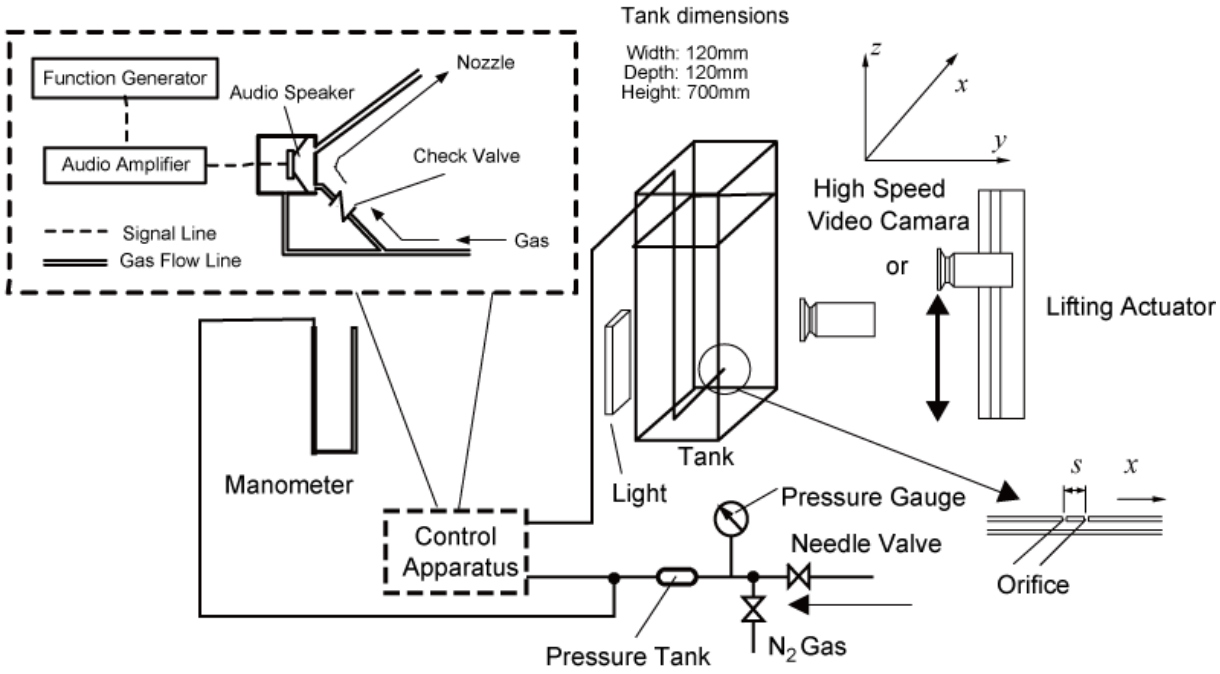

Fig.1 Experimental apparatus on bubble motion visualization

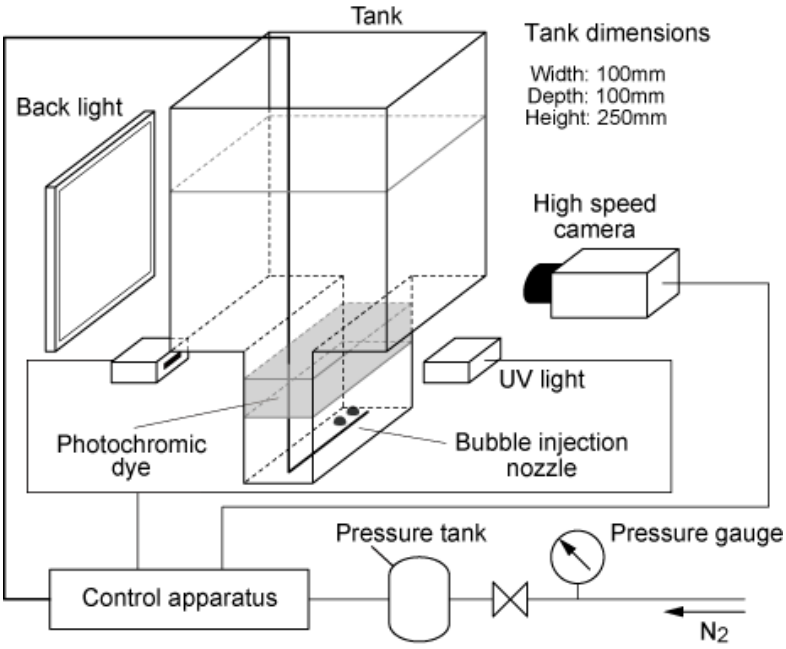

Fig.2 Experimental apparatus on bubble wake visualization

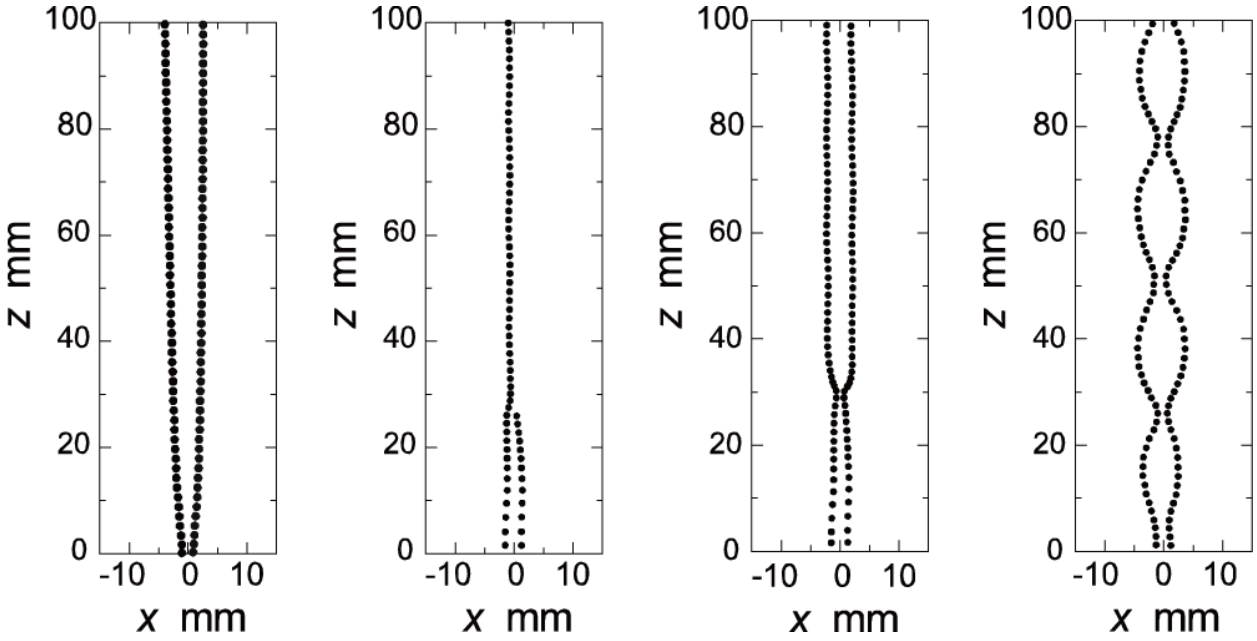

(a) *s*=1.8 mm *Re*=16 (b) *s*=2.2 mm *Re*=209 (c) *s*=2.2 mm *Re*=221 (d) *s*=2.5 mm *Re*=361

Fig.3 Trajectory of a pair of bubbles rising in a quiescent liquid

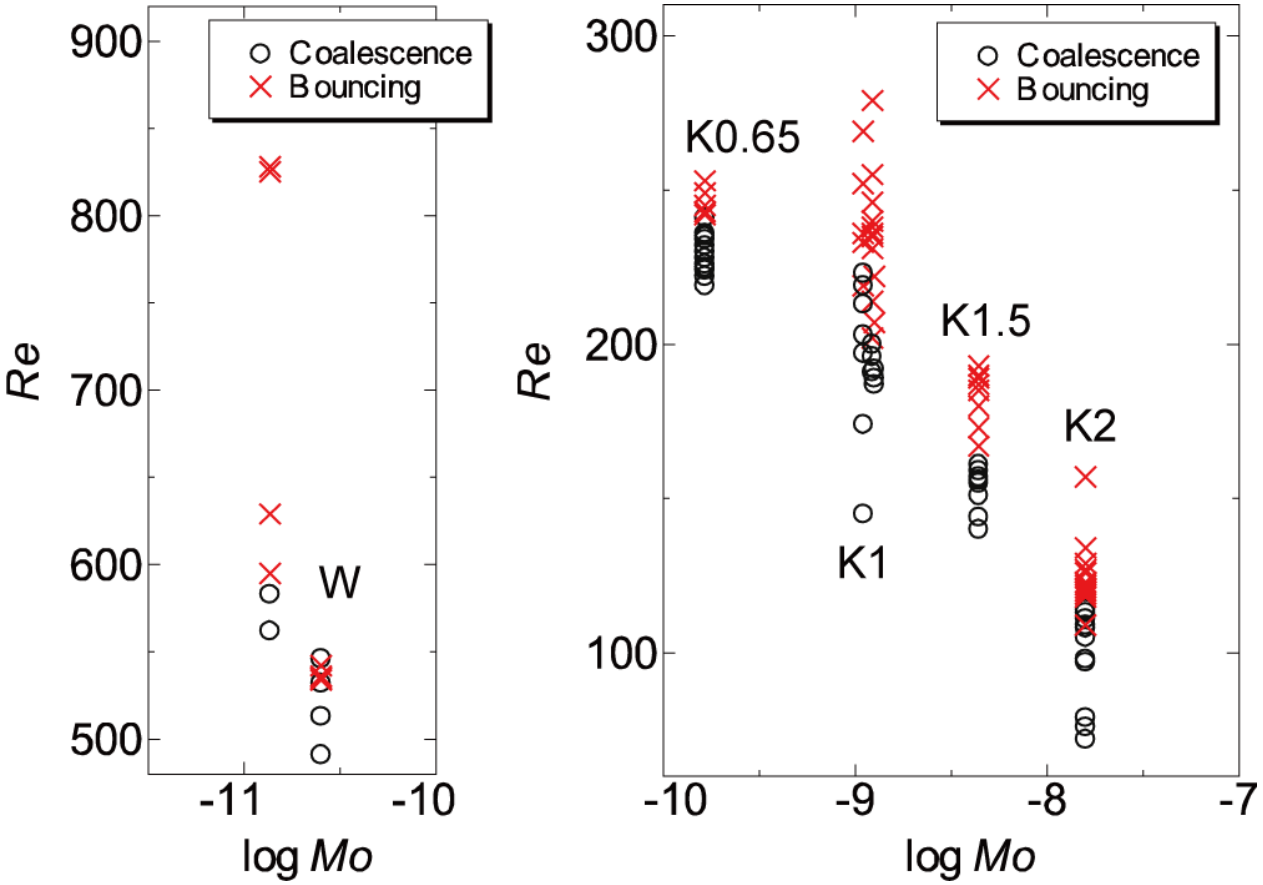

Fig.4 Criteria of coalescence of *Re* (W:Water, K:Silicone oil)

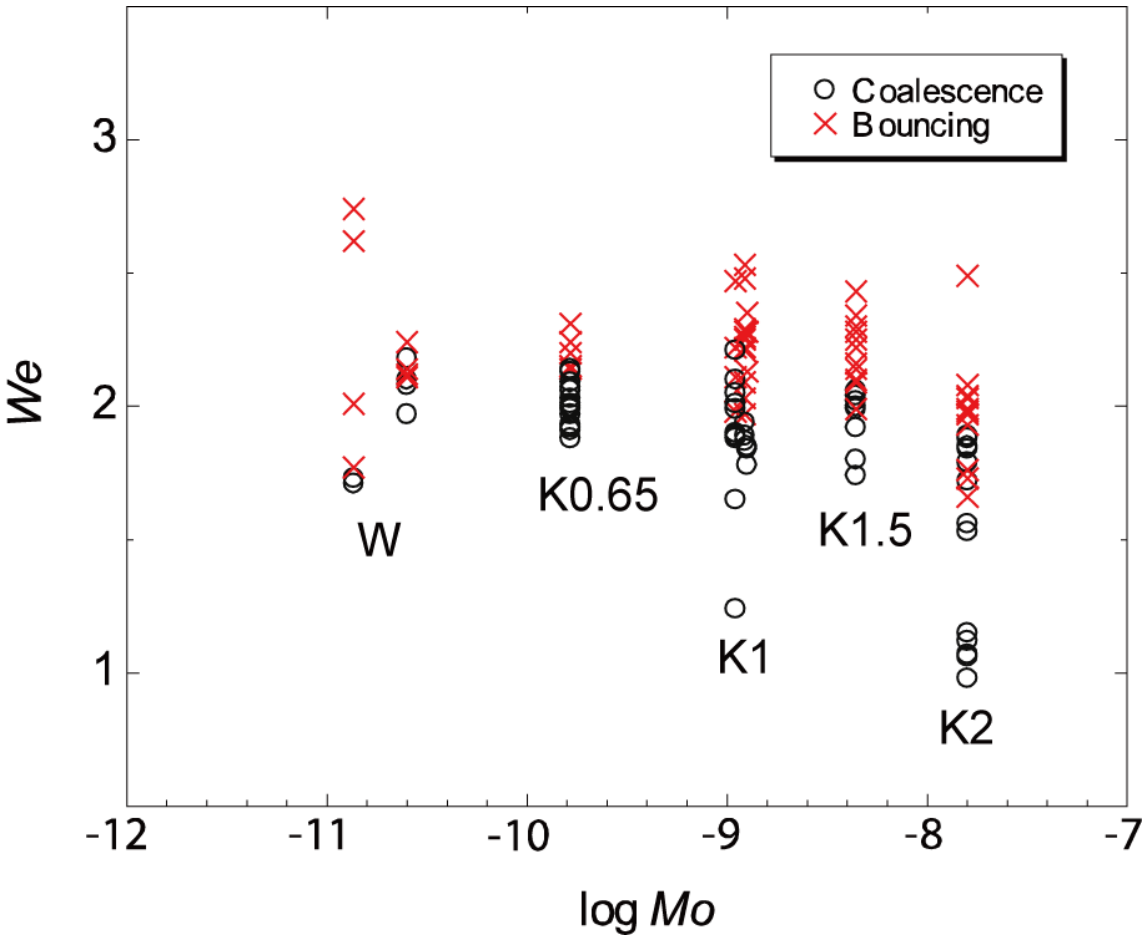

Fig.5 Criteria of coalescence of *We* (W:Water, K:Silicone oil)

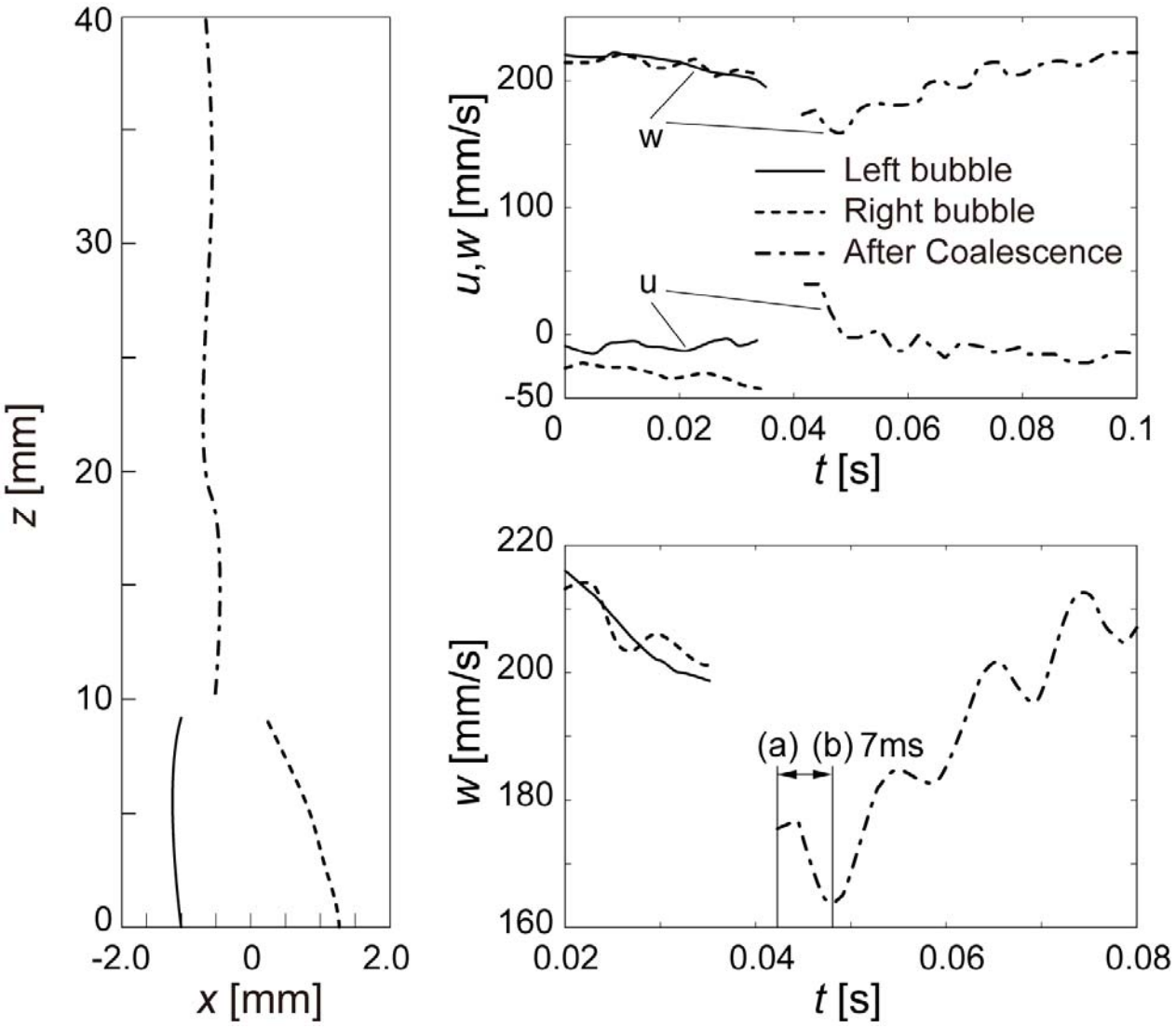

Fig.6 Trajectory and vertical/horizontal velocity of a pair of bubbles (pattern 1)

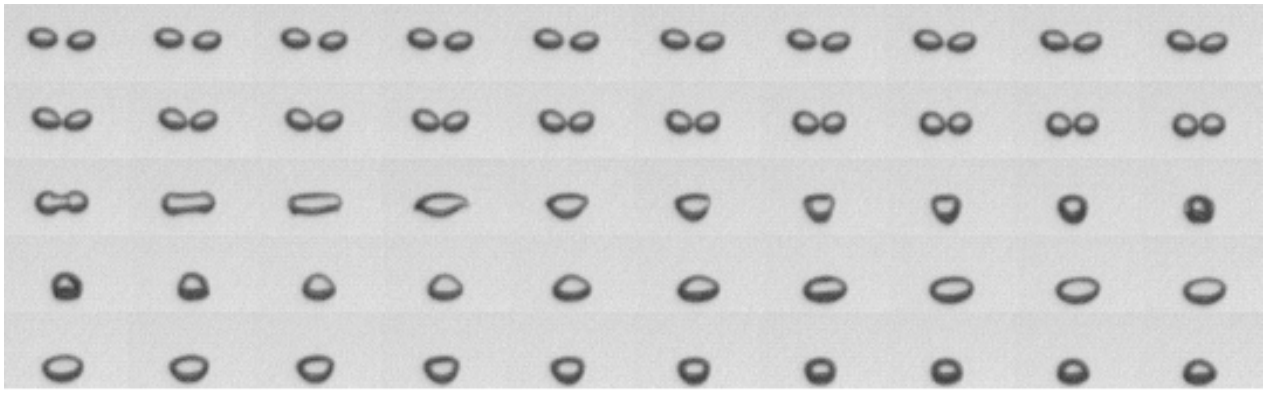

Fig.7 Shape change of coalescence bubble from left to right, line by line to the bottom (Δt=0.5msec)

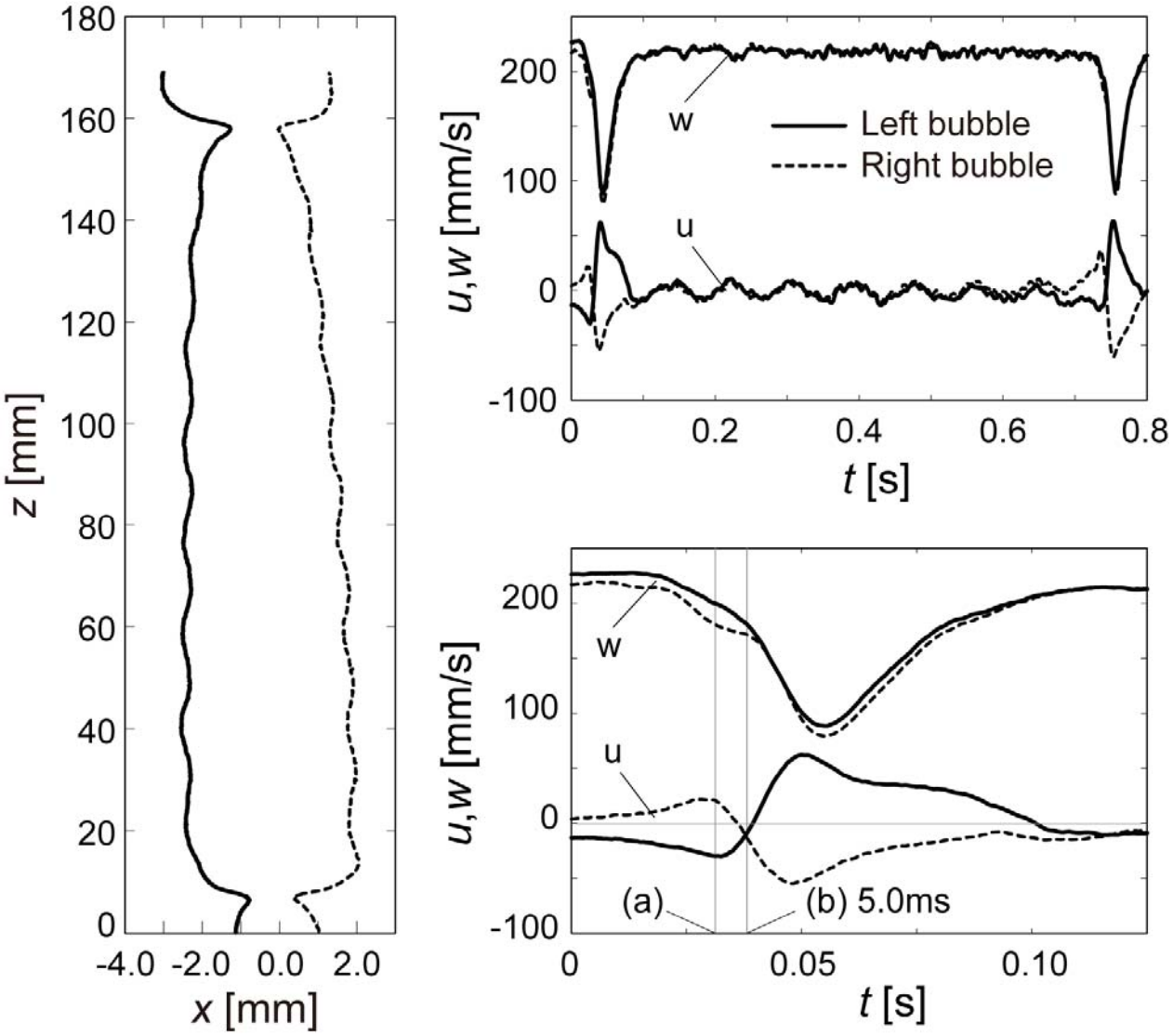

Fig.8 Trajectory and vertical/horizontal velocity of a pair of bubbles (pattern 2)

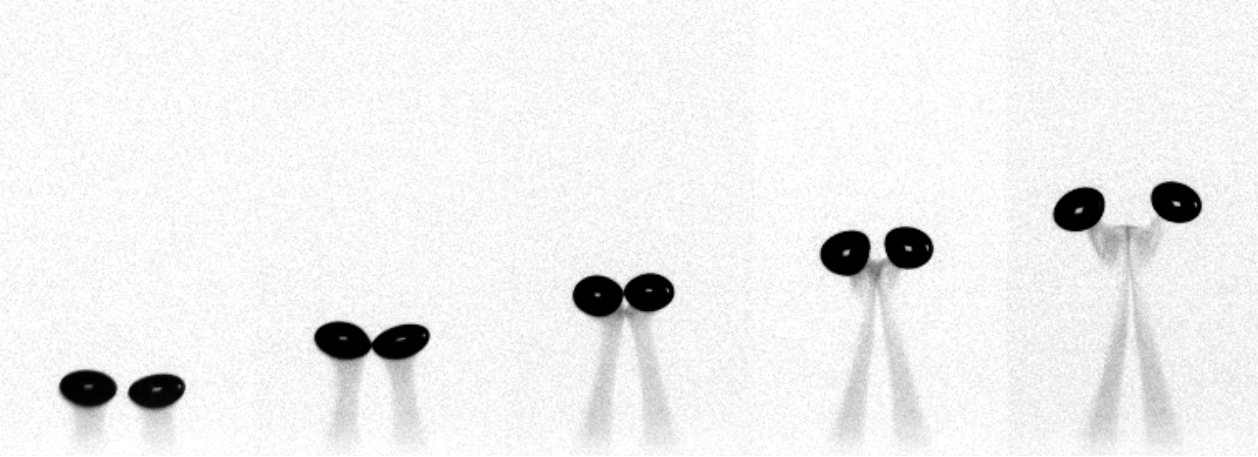

(a) type1

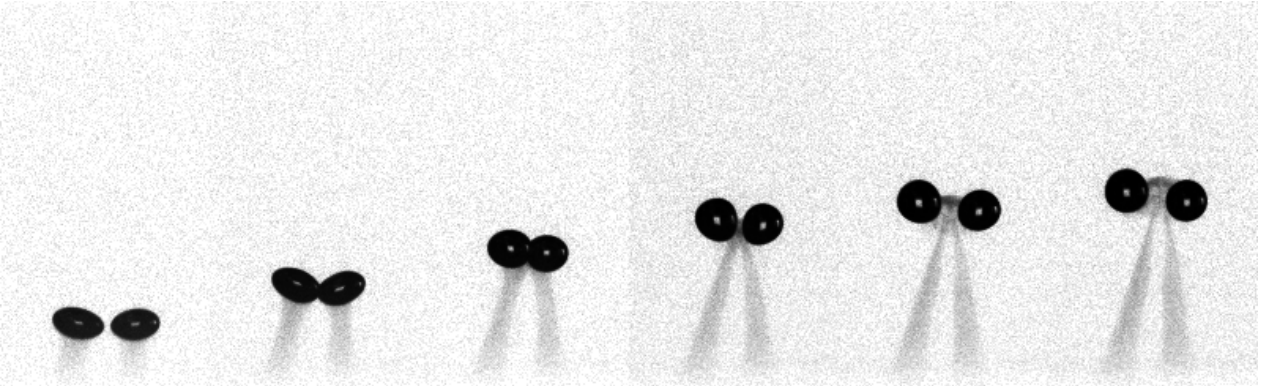

(b) type2

Fig.9 Wake of bouncing of bubbles (Δt=4msec)

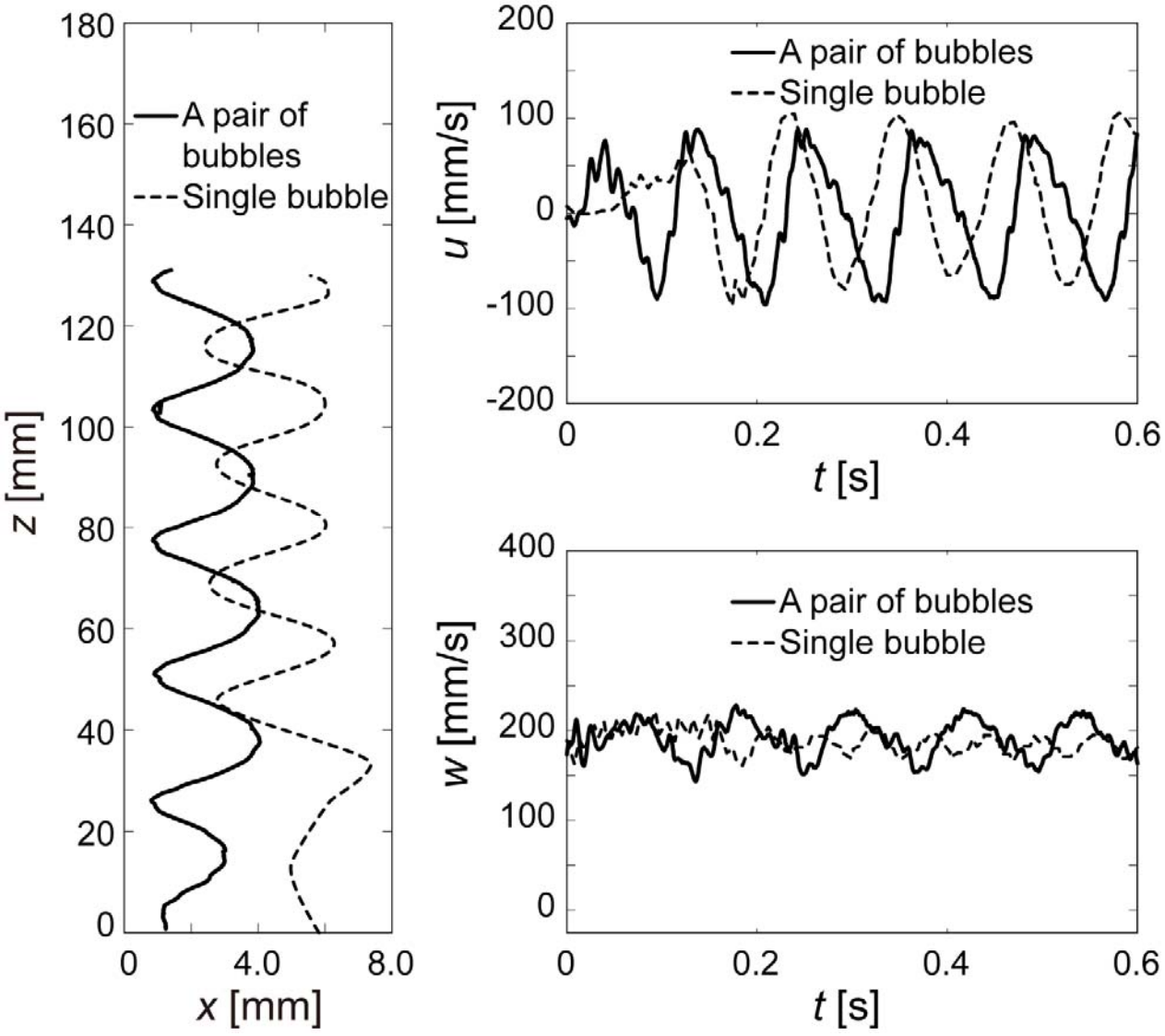

Fig.10 Trajectory and vertical/horizontal velocity of a pair of bubbles (pattern 3)

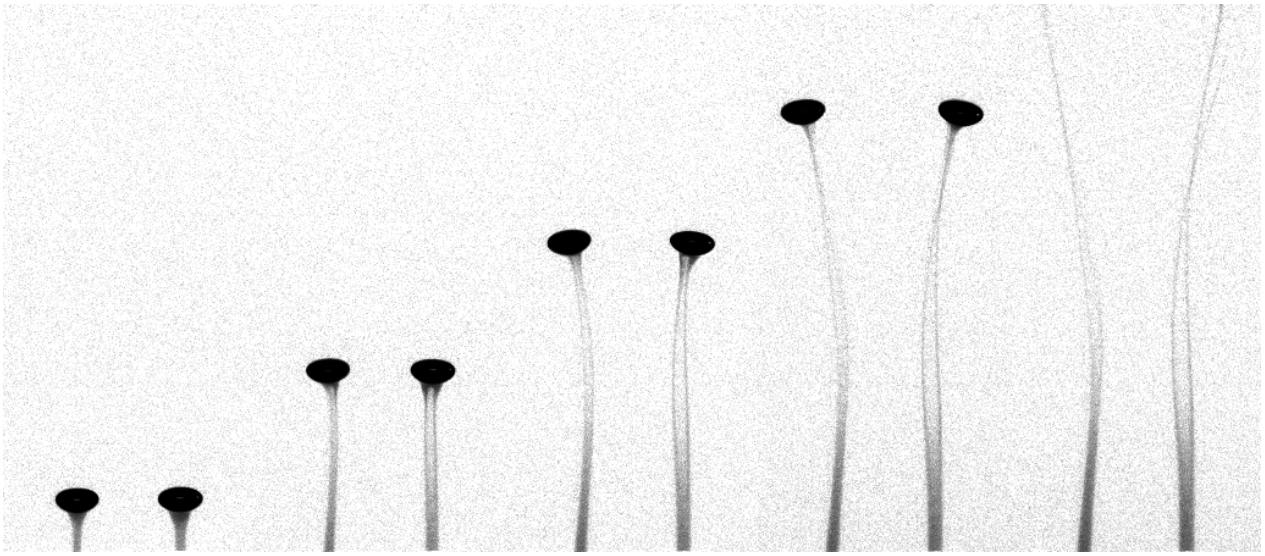

(a) type1

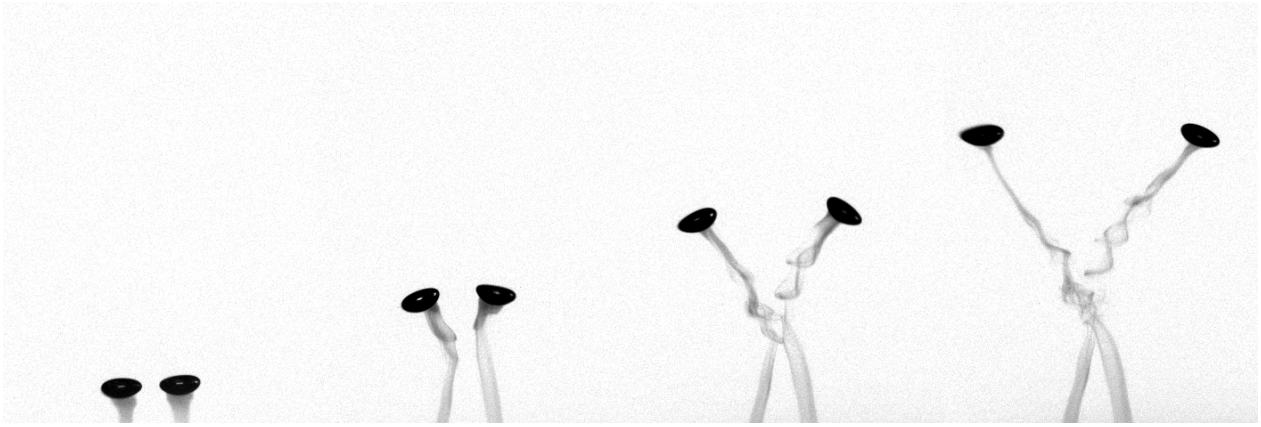

(b) type2

Fig.11 Wake of pair of bubbles (Δt=10msec)

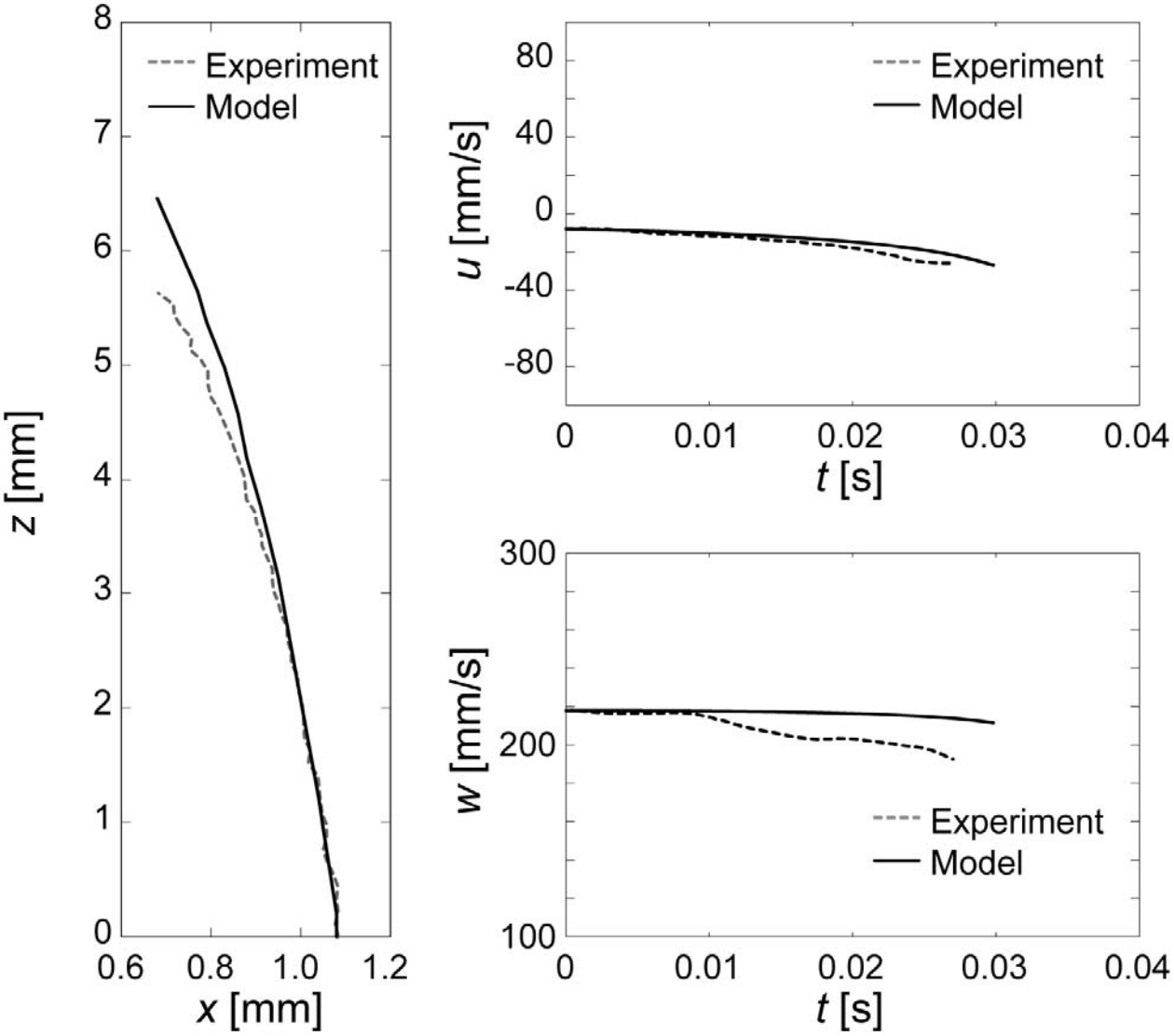

Fig.12 Comparison of experiment with model (pattern 1)

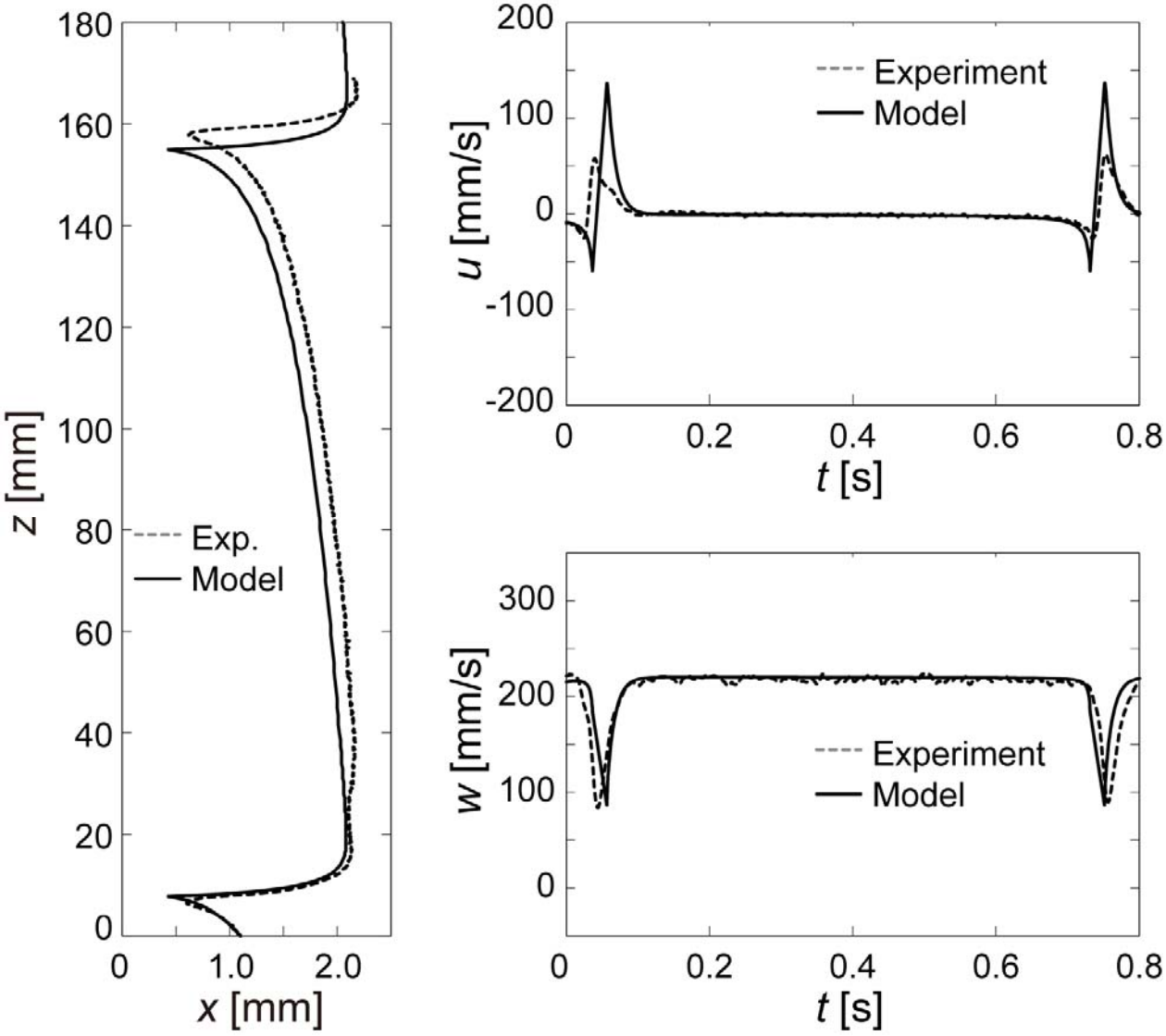

Fig.13 Comparison of experiment with model (pattern 2)

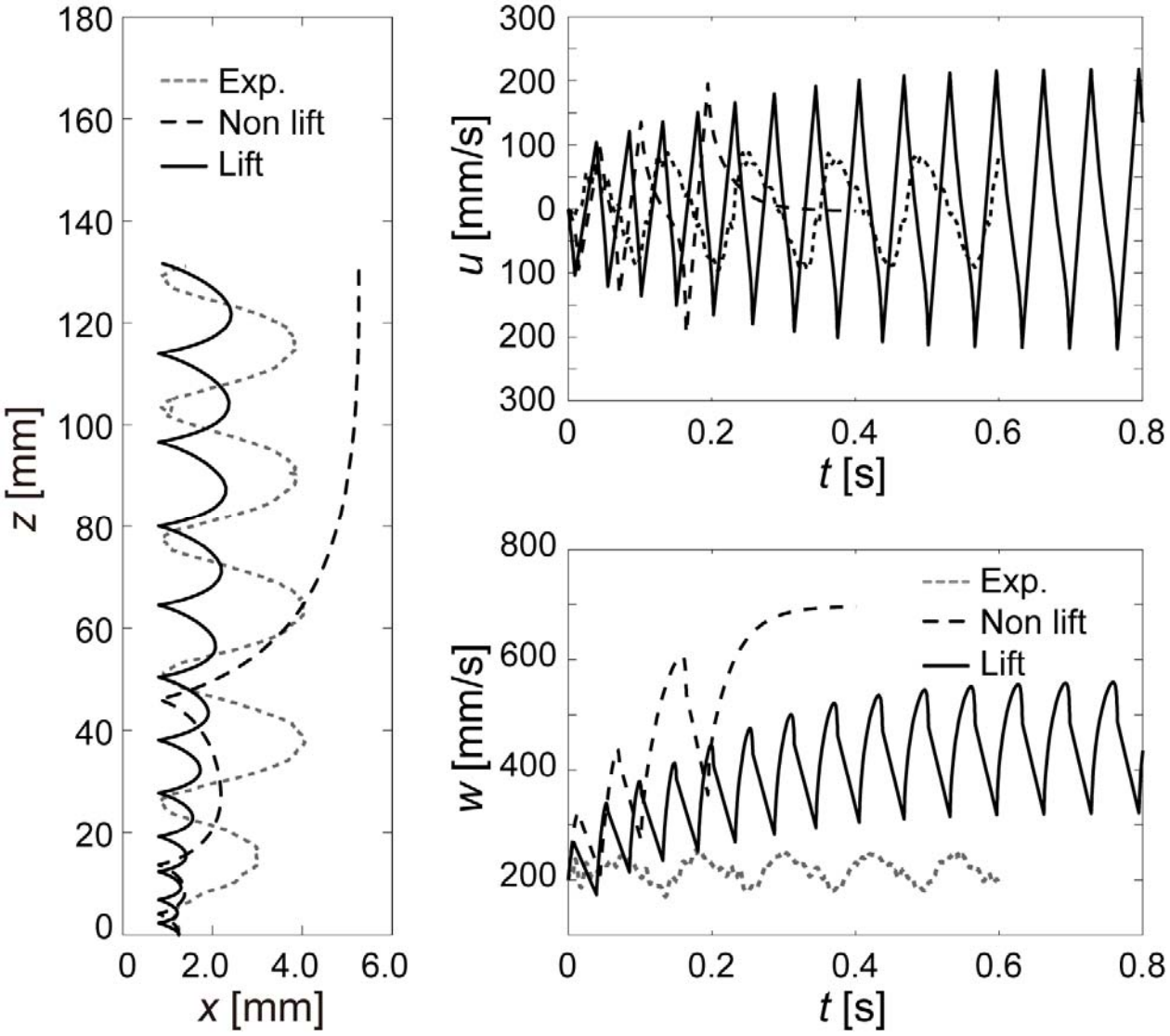

Fig.14 Comparison of experiment with model (pattern 3)

Table 1 Properties of liquid (W: Water, K: Silicone oil, M: Silicone oil with photochromic dye mixture)

	W	K0.65	K1	K1.5	K2	K5	K10	M
ρ kg/m^3	996-998	758	817-820	849	871	911	938	812
ν cSt	0.85-1.06	0.63	1.00-1.06	1.42	1.97	4.63	10.33	1.17
σ mN/m	71.6-73.0	15.9	16.9	17.7	18.3	19.7	20.1	16.7
Mo	1.36-3.14	1.65	1.10-1.49	4.41	1.59	4.46	1.14	2.11
	$\times 10^{-11}$	$\times 10^{-10}$	$\times 10^{-9}$	$\times 10^{-9}$	$\times 10^{-8}$	$\times 10^{-7}$	$\times 10^{-5}$	$\times 10^{-9}$

Table 2 Experimental parameters of each bubble pattern

	r_{eq}	s	Re	U_T
	[mm]	[mm]	[-]	[mm/s]
Pattern 1	0.51	1.43	163	≒195
Pattern 2	0.54	1.1	194	≒220
Pattern 3	0.89	1.25	291	≒200
Pattern 3'	0.83	-	272	≒200

FIGURE CAPTIONS (APPENDIX)

Figure A1. Separate distance and approach velocity of a pair of bubbles

Figure A2. Images at the collision of bubbles (Δt=2.5msec)

Figure A3. Approach velocity before encounter

Figure A4. Separate distance and rising velocity of a pair of bubbles

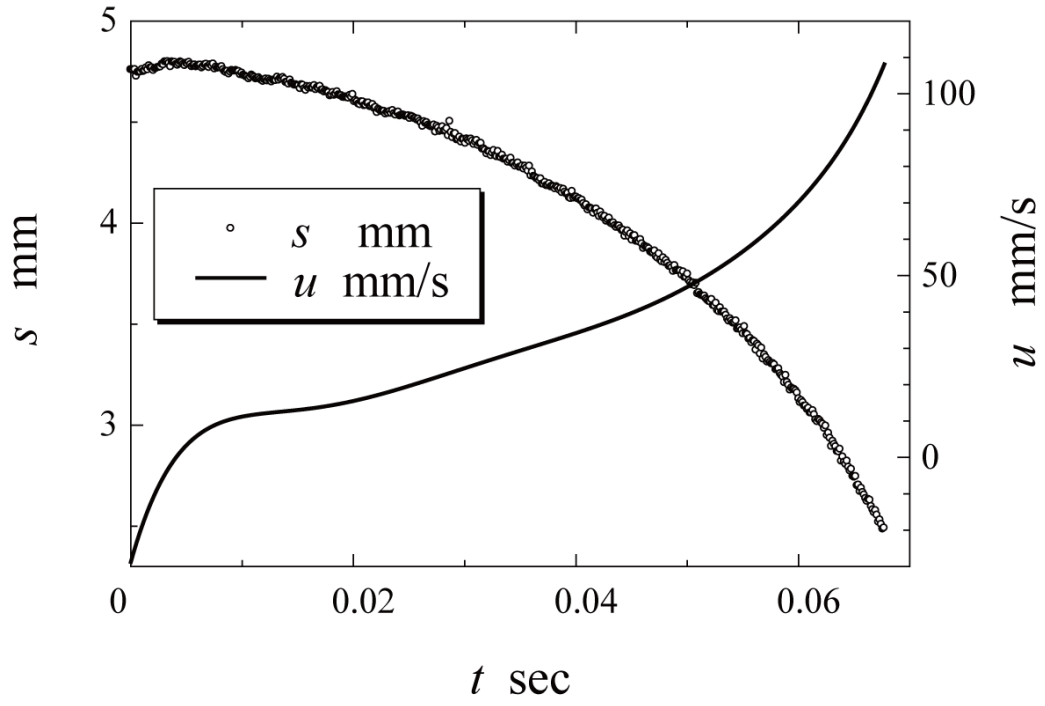

Fig.A1 Separate distance and approach velocity of a pair of bubbles

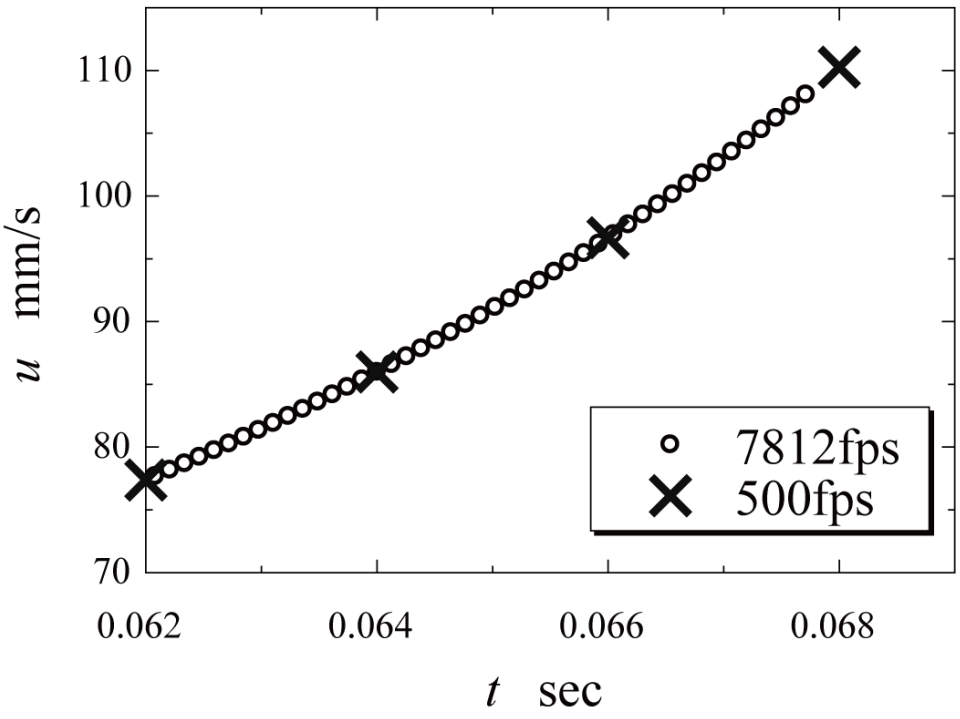

Fig.A2 Images at the collision of bubbles (Δt=2.5msec)

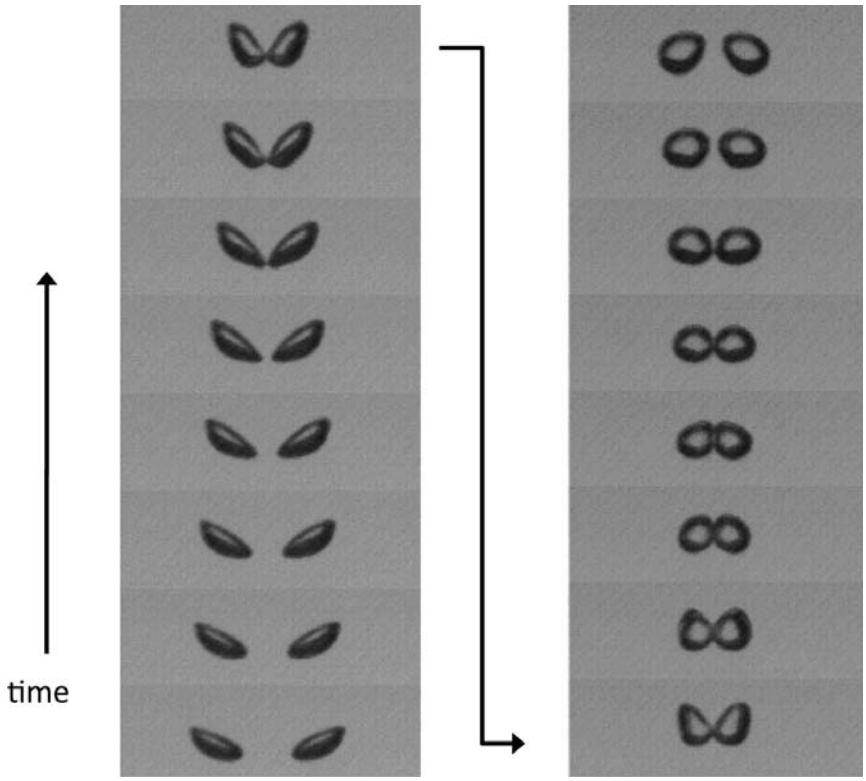

Fig.A3 Approach velocity before collision

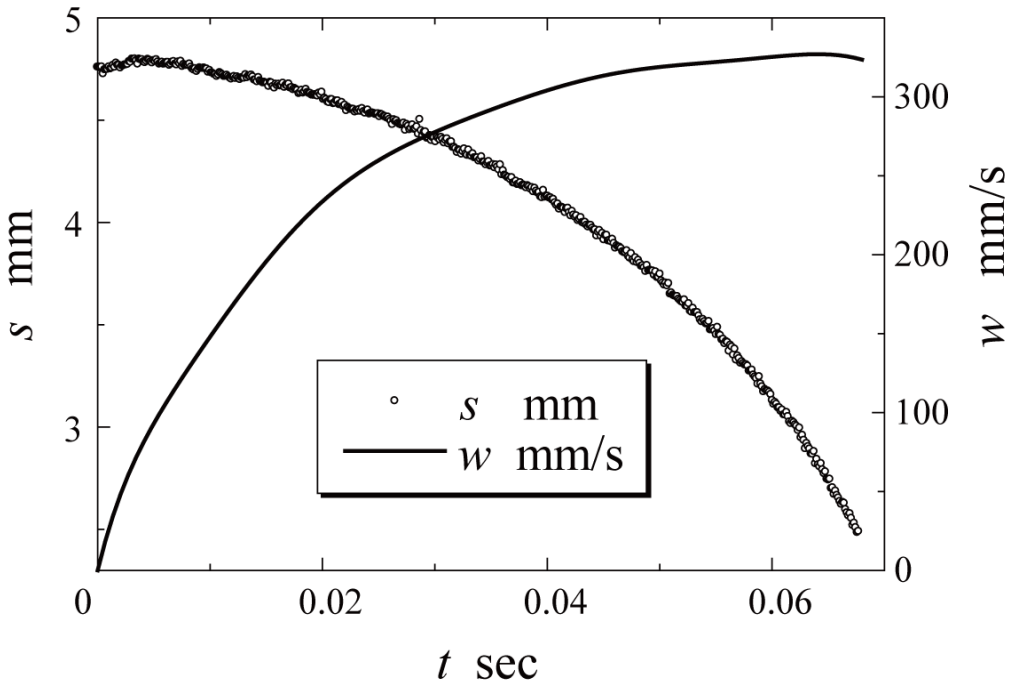

Fig.A4 Separate distance and rising velocity of a pair of bubbles